Synthesis and optical properties of luminescent core-shell structured silicate and phosphate nanoparticles

Sofia Dembski[1]*, Sabine Rupp[1], Moritz Milde[1], Carsten Gellermann[1], Marcel Dyrba[2], Stefan Schweizer[2], Miroslaw Batentschuk[3], Andres Osvet[3], Albrecht Winnacker[3]

[1]Fraunhofer Institute for Silicate Research ISC, Neunerplatz 2, D-97082 Wuerzburg, Germany

[2]Center for Innovation Competence SiLi-nano®, Martin Luther University of Halle-Wittenberg, Karl-Freiherr-von-Fritsch-Str. 3, D-06120 Halle (Saale), Germany, and Fraunhofer Center for Silicon Photovoltaics, Walter-Huelse-Str. 1, D-06120 Halle (Saale), Germany

[3]Department of Materials Science and Engineering 6, University of Erlangen-Nuremberg, Martensstr. 7, D-91058 Erlangen, Germany

*To whom correspondence should be addressed. sofia.dembski@isc.fraunhofer.de, Fraunhofer Institute for Silicate Research ISC, Neunerplatz 2, D-97082 Wuerzburg, Germany Tel.: +499314100-516, Fax:+499314100-399.

Abstract:

Monodisperse, luminescent core-shell structured inorganic nanoparticles were synthesized by sol-gel technology. They exhibit an amorphous SiO_2 core and a crystalline luminescent shell. Zn_2SiO_4:Mn^{2+} and $Ca_{10}(PO_4)_6OH$:Eu^{3+} shell materials are investigated. The influence of the doping concentration on optical and structural properties was studied. The resulting nanoparticles were characterized by X-ray diffraction analysis, transmission electron microscopy, inductively coupled plasma optical emission spectrometry, and photoluminescence spectroscopy.

Keywords: nanophosphor, luminescent core-shell nanoparticles, Zn_2SiO_4, hydroxyapatite

1. Introduction

In recent years, a great deal of interest has been focused on the fabrication and characterization of rare-earth based inorganic luminescent nanoparticles (NPs). Potential fields of application are, for example, optics and optoelecronics, pharmaceutics or biological and medical diagnostics [1-3]. Just like semiconductor NPs (quantum dots, QDs), rare-earth doped NPs are highly photostable, exhibit long luminescence lifetimes and narrow emission bands. In contrast to QDs, however, the emission color is not dependent on the particle size. It can be adjusted by the choice of the host material and dopants and their combination. The luminescence intensity is dependent on the concentration of doping ions, the crystal structure of the host material, and the degree of crystallinity [4]. The high chemical stability and bright luminescent performance of these NPs make them potentially suitable for biological labeling [3].

During the last decade, several strategies such as co-precipitation, hydrothermal reaction, sol-gel synthesis or the microemulsion method have been developed to produce highly luminescent inorganic NPs of adjustable particle morphology and size [1,5,6]. In this respect, an elegant synthesis strategy to prepare luminescent inorganic NPs of high quality is the fabrication of core-shell-structured NPs according to the modified solution-based Pechini-type process [7-10]. To this end, non-aggregated, spherical silica cores are coated with phosphor layers by sol-gel technology. Subsequent annealing of the samples results in the formation of core-shell structured particles. These particles exhibit an amorphous core and a crystalline luminescent shell. Their structure, size, size distribution, and composition can easily be controlled to tailor their chemical and physical properties. In previous articles [9,10], we reported on the synthesis of $SiO_2/Zn_2SiO_4:Mn^{2+}$ and $SiO_2/Ca_{10}(PO_4)_6OH:Eu^{3+}$ core-shell NPs with diameters below 100 nm. We have identified the relevance of synthesis parameters such

as pH value or annealing temperature for the formation of a crystalline shell around the SiO_2 core. It has been established that the formation of a crystalline hydroxyapatite (HAp, $Ca_{10}(PO_4)_6OH$) layer on the surface of SiO_2 cores is possible at pH above 6. However, the crystal structure and optical properties of the zinc silicate shell can be tuned by selected annealing conditions. Annealing of the coated particles at 800 °C causes the formation of a Mn^{2+}-doped ZnO shell. The α-Zn_2SiO_4 (willemite) phase starts to form through annealing at 900 – 1100 °C. Due to their chemical and physical properties, both NP systems might be good candidates for the manufacturing of luminescent markers in biological and medical diagnostics.

The object of this study is to investigate the effect of the doping concentration on the optical and structural properties of $SiO_2/Zn_2SiO_4:Mn^{2+}$ and $SiO_2/Ca_{10}(PO_4)_6OH:Eu^{3+}$ core-shell NPs. The characterization of the resulting NPs is done by transmission electron microscopy (TEM), X-ray diffraction (XRD) analysis, inductively coupled plasma optical emission spectrometry (ICP-OES), and photoluminescence (PL) spectroscopy.

2. Experimental

2.1. Materials

The starting materials for the preparation of the core-shell NPs were ethanol (CSC Jaeklechemie), tetraethoxysilane $Si(OC_2H_5)_4$ (TEOS, 98 %, Sigma-Aldrich), ammonium hydroxide solution in water (25 %, Fluka), citric acid monohydrate (98 %, Aldrich), polyethylene glycol (PEG, mw = 10000, Fluka), nitric acid (10 mol/L, Merck), calcium nitrate tetrahydrate $Ca(NO_3)_2 \cdot 4H_2O$ (99 %, Sigma-Aldrich), diammonium hydrogen phosphate $(NH_4)_2HPO_4$ (99 %, Sigma-Aldrich), europium chloride hexahydrate $EuCl_3 \cdot 6H_2O$ (99.9 %, Aldrich), zinc acetate dihydrate $Zn(O_2C_2H_3)_2 \cdot 2H_2O$ (98 %, Sigma-Aldrich), and manganese acetate $Mn(O_2C_2H_3)_2$ (98 %, Sigma-Aldrich). All chemicals were used as received without any further purification.

2.2. Nanoparticle preparation

SiO_2/Zn_2SiO_4: Mn^{2+} and $SiO_2/Ca_{10}(PO_4)_6OH:Eu^{3+}$ core-shell nanoparticles were synthesized as described by Dembski et al. [9,10].

2.2.1. Preparation of $SiO_2/Ca_{10}(PO_4)_6OH:Eu^{3+}$ core-shell nanoparticles

In a typical reaction, $Ca(NO_3)_2 \cdot 4H_2O$, $EuCl_3 \cdot 6H_2O$ and $(NH_4)_2HPO_4$ were dissolved in a mixture of ethanol and water (ethanol/water = 1/3 in volume) in the presence of citric acid monohydrate. The molar ratio of metal ions to citric acid was 1/2. The pH of 8.6 was adjusted by the addition of an ammonium hydroxide solution in water. After the addition of PEG, the resulting mixture (final concentration 0.05 g/ml) was stirred and ultrasonically treated until the starting materials were dissolved. A dispersion of SiO_2 cores (prepared according to a modified Stoeber method) in ethanol was added to the solution of metal salts and stirred for 3 h at RT [11,12]. The resulting core-shell NPs were collected by centrifugation, redispersed in water, freeze-dried and annealed at 800 °C.

2.2.2. Preparation of $SiO_2/Zn_2SiO_4:Mn^{2+}$ core-shell nanoparticles

For the surface coating of SiO_2 cores with a Mn^{2+}-doped zinc silicate shell, $Zn(O_2C_2H_3)_2 \cdot 2H_2O$ and $Mn(O_2C_2H_3)_2$ were dissolved in a mixture of ethanol and water in the presence of nitric acid (ethanol/water = 8/1 in volume). After the addition of citric acid monohydrate (molar ratio metal ions/citric acid = 1/2) and PEG (final concentration 0.05 g/ml), the resulting mixture was stirred and ultrasonically treated until the starting materials were dissolved. The following coating steps were conducted as described in 2.2.1. The coated particles were annealed at 900 °C and at 1100 °C, respectively.

2.3. Characterization

The morphology of the core-shell NPs was studied by transmission electron microscopy using a Zeiss EM 10 TEM with an acceleration voltage of 80 keV. Samples were prepared by dipping 200 mesh copper grids coated with a thin carbon film (Quantifoil Micro Tools GmbH) into an aggregate-free NP dispersion. NP sizes were determined by the measurement tools of the software ImageC from IMTRONIC GmbH by binarization of the images and an estimation of the mean particle radius. A diffraction grating (2160 lines/mm) was used to calibrate the magnification. Generally, 100 – 200 nanoparticles were analyzed. The crystallinity of the powder samples was analyzed using a Philips PW 1152.

The Eu^{3+}-related emission and excitation spectra were recorded using a xenon lamp (450 W), a double monochromator (Horiba Jobin Yvon Gemini-180) for excitation, a monochromator with 0.32 m focal length (Horiba Jobin Yvon iHR320) for emission, and a cooled photomultiplier (Hamamatsu R2658P) for detection. The samples were pressed into tablets of about 10 mm in diameter.

The PL spectra of Mn^{2+}-doped samples were measured at room temperature and at 18 K under 260 nm excitation. The samples were irradiated with a 75 W Xe lamp through an infrared-blocking filter and a 260 nm interference filter. The emission was dispersed with a 0.6 m Jobin-Yvon monochromator at a resolution of 0.5 nm and detected with a photomultiplier with lock-in technique. The PL decay curves were measured by exciting the samples with a pulsed Xe lamp through a 260 nm interference filter and detecting the emission at its maximum wavelength through a 0.1 m monochromator. The signal was detected with a photomultiplier and recorded by a digital oscilloscope. The pulse width of the lamp (4 µs) was sufficiently short to match the typical millisecond lifetimes of the Mn^{2+} emission.

3. Results and discussion

3.1. Synthesis and characterization of core-shell structured luminescent phosphate and silicate nanoparticles

The luminescent $SiO_2/Zn_2SiO_4:Mn^{2+}$ and $SiO_2/Ca_{10}(PO_4)_6OH:Eu^{3+}$ core-shell NPs were prepared as described previously according to a procedure that is based on the Pechini sol-gel process [9,10]. The coating of silica cores (d = 46 ± 6 nm) with a luminescent shell was carried out in two steps: wet-chemical coating of silica cores and annealing of coated NPs. The amount of starting materials was calculated to yield colloids with a shell thickness of about 5 nm. The concentration of Mn^{2+} ions was varied between 0 mol% and 20 mol% (0 mol%, 0.1mol%, 1 mol%, 5 mol%, 20 mol%) referring to Zn^{2+} in Zn_2SiO_4. The concentration of Eu^{3+} ions was varied between 0 mol% and 2.5 mol% (0%, 0.5%, 2.5 mol%) referring to Ca^{2+} in HAp. The overall molar ratio (Ca+Eu) to phosphate (Ca+Eu)/P was adjusted to be 1.67 (assuming that Eu^{3+} ion substitutes for Ca^{2+}). The starting materials for the shell were dissolved in a water/ethanol solution in the presence of citric acid as chelating agent and polyethylene glycol (PEG) as cross-linking agent. Network formation after chelation of metal ions leads to their stabilization and to a homogeneous distribution of the shell material onto the silica core surface. Finally, coated NPs were lyophilized and annealed at 800 °C for the formation of the calcium phosphate shell and at 900 °C or at 1100 °C, respectively, for the $Zn_2SiO_4:Mn^{2+}$ shell.

After coating of the silica cores with an inorganic layer, the resulting core-shell NPs still keep the spherical form (see insets in Figure 1 and Figure 2). However, in contrast to pure silica cores, we did not observe a growth in the diameter of core-shell NPs. This might be caused by the shrinkage of the silica core upon annealing at high temperatures, as reported by others [8]. The amount of incorporated Ca^{2+} determined by ICP-OES is about 37 – 51 % of the Ca^{2+}-educt. Respectively, about 70 – 86 % of Eu^{3+} precursor was incorporated into the calcium phosphate layer. These results imply that the used calcium and europium precursors do not completely react to the shell. The elementary analysis of $SiO_2/Zn_2SiO_4:Mn^{2+}$ core-shell NPs brought similar results. A maximum of 58 % of the Zn^{2+} precursor was converted into a shell. For the samples coated with zinc silicate, only 10 % of the Mn^{2+} precursor were incorporated.

Obviously, in both particle systems the effective layer is thinner than expected. That explains the difficulty to verify the outer shell by TEM. The mechanism of incorporating doping ions into the host materials of the shell is presently being studied in detail [13].

Figure 1 shows selected XRD patterns of $SiO_2/Ca_{10}(PO_4)_6OH:Eu^{3+}$ core-shell NPs doped with 2.5 mol% Eu^{3+}. Other samples (without doping and with 0.5 mol% Eu^{3+}) exhibited the same tendency.

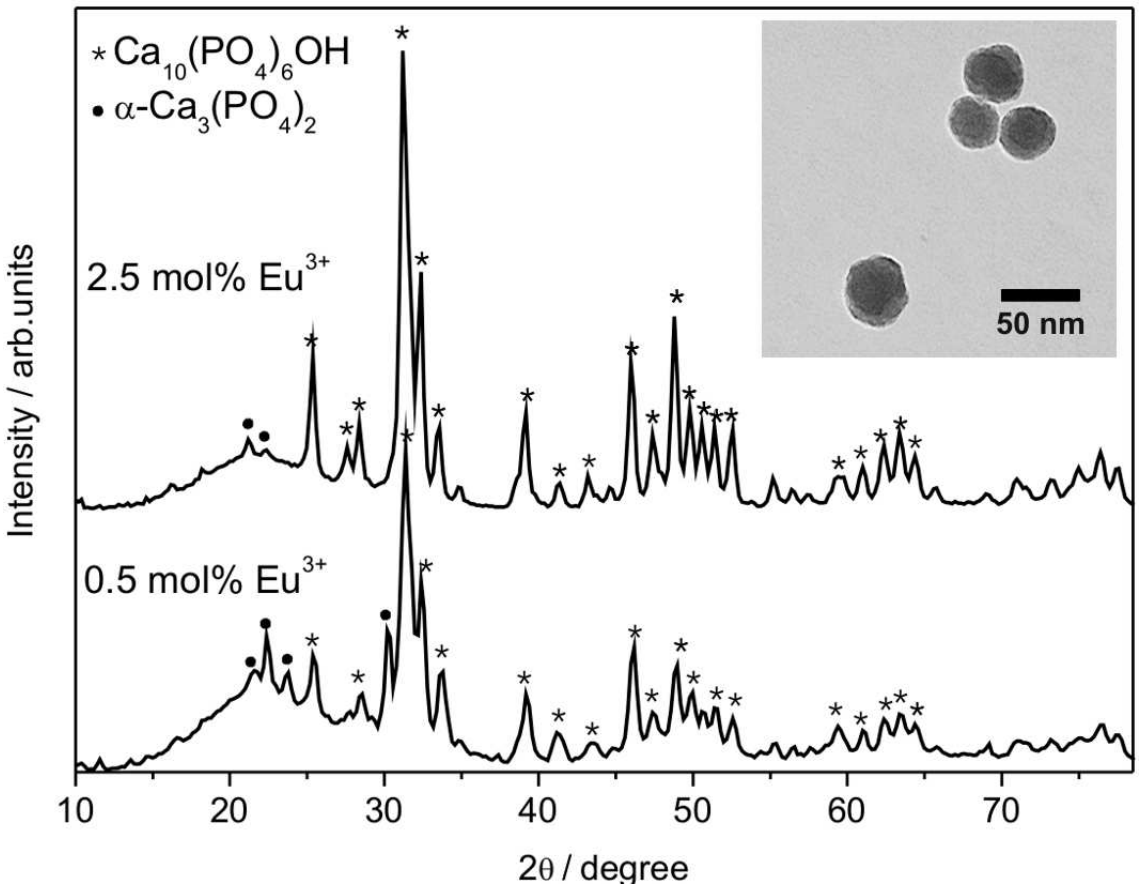

Figure 1. XRD patterns of $SiO_2/Ca_{10}(PO_4)_6OH:Eu^{3+}$ core-shell NPs doped with 2.5 mol% Eu^{3+}. The phase composition was checked by means of JCPDS reference patterns for $Ca_{10}(PO_4)_6OH$ (PDF Ref. 74-0565), α-$Ca_3(PO_4)_2$ (PDF Ref. 29-0359). Inset: TEM image of $SiO_2/Ca_{10}(PO_4)_6OH:Eu^{3+}$ core-shell NPs.

The phase analysis of the XRD patterns indicated that the main crystalline phase is HAp. Moreover, a small amount of α-tricalcium phosphate (α-TCP) was detected in all samples. The broad reflection at about $2\theta = 22°$ certified the presence of the amorphous SiO_2 core and

is typical for all core-shell NPs [7–10]. According to the ICP-OES results, the (Ca+Eu)/P ratio of the samples was calculated to be 1.58 (NPs sample doped with 0.5 mol%) and 1.68 (NPs sample doped with 2.5 mol%) which is consistent with a presence of a HAp (1.67) und α-TCP (1.50) mixture, as reported by others [14,15]. The presented results demonstrate the possibility of the preparation of $SiO_2/Ca_{10}(PO_4)_6OH:Eu^{3+}$ core-shell NPs doped with various amounts of doping ions without any change of the shell crystal structure.

$SiO_2/Zn_2SiO_4:Mn^{2+}$ core-shell NPs were also examined by means of XRD. There is no difference between the individual NP samples doped with different amounts of Mn^{2+}. But a difference was observed between doped and undoped samples in the diffraction patterns, which are depicted in Figure 2.

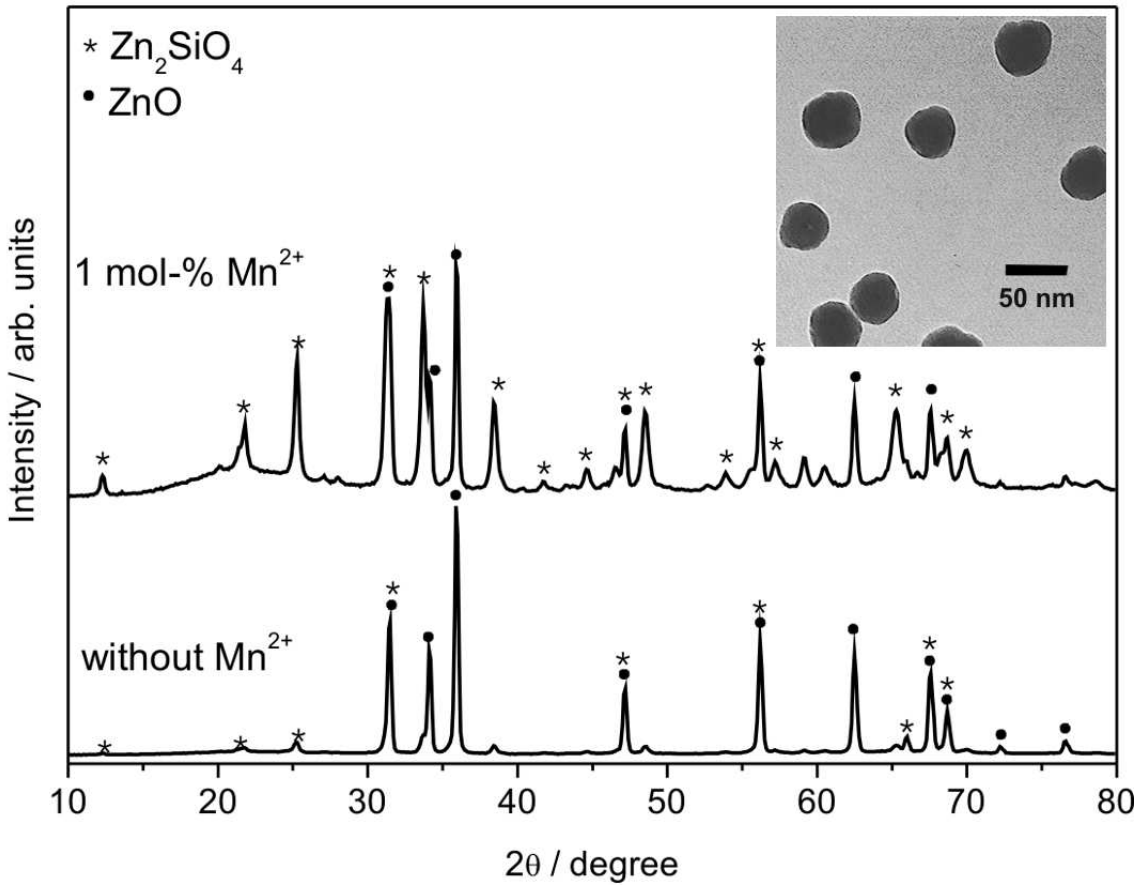

Figure 2. XRD patterns of SiO_2/Zn_2SiO_4 core-shell NPs doped with 1 mol% Mn^{2+} and without doping annealed at 900°C. The phase composition was checked by means of JCPDS reference patterns for α-Zn_2SiO_4 (PDF Ref. 37-1485) and ZnO (PDF Ref. 36-1451). Inset: TEM image of $SiO_2/Zn_2SiO_4:Mn^{2+}$ core-shell NPs (the doping concentration of Mn^{2+} 1 mol%).

Without Mn^{2+}-doping the ZnO phase is predominant and signals for α-Zn_2SiO_2 are only slightly formed. By increasing the concentration of Mn^{2+} up to 1 mol% and higher, the intensity of Zn_2SiO_4 signals also increases. Chakradhar et al. [16] described the same tendency in the formation of crystalline Zn_2SiO_2:Mn^{2+}. Possibly, the presence of Mn^{2+} ions in the reaction mixture promotes the formation of the zinc silicate crystal phase.

3.2. Site-selective photoluminescence spectroscopy on $SiO_2/Ca_{10}(PO_4)_6OH:Eu^{3+}$ core-shell nanoparticles

Figure 3 shows the emission spectrum of a 2.5 mol% Eu^{3+}-doped sample (curve a). The excitation energy was 29,412 cm^{-1} (340 nm). The main emission lines at 17,460 cm^{-1}, 16,680 cm^{-1}, and 16,000 cm^{-1} can be assigned to $^5D_0 \rightarrow {}^7F_J$ transitions of Eu^{3+} with J = 0, 1, and 2, respectively [17]. Upon excitation at 25,350 cm^{-1} (394.5 nm) more emission bands appear (Figure 3, curve b). The line groups at 15,330 cm^{-1} and 14,230 cm^{-1} belong to J = 3 and 4, respectively.

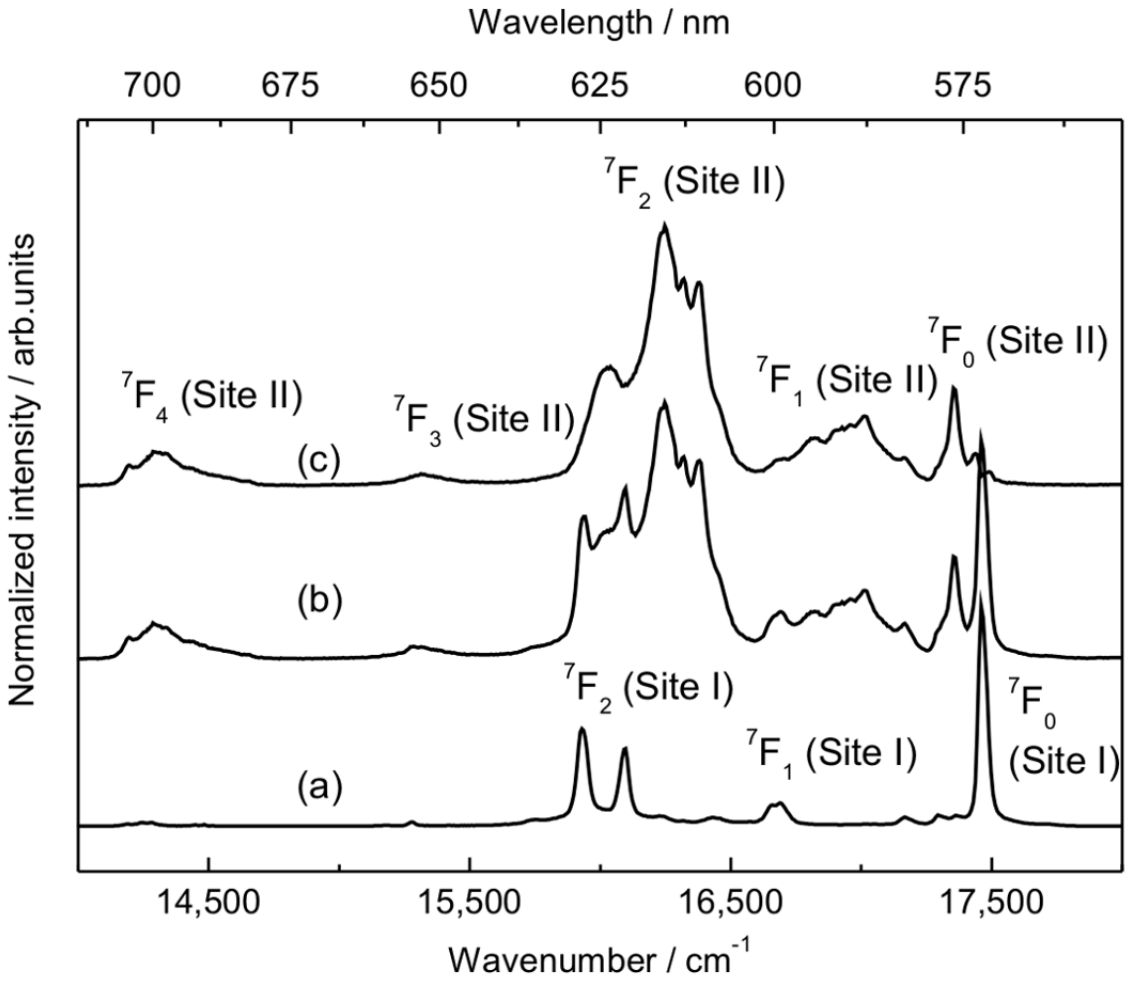

Figure 3. Normalized PL spectra of $SiO_2/Ca_{10}(PO_4)_6OH:Eu^{3+}$ core-shell NPs sample (the doping concentration of Eu^{3+} is 2.5 mol%) excited at (a) 29,412 cm^{-1} (340.0 nm – site I) and (b) 25,348 cm^{-1} (394.5 nm – site I and II). Curve (c) is the difference spectrum between curve (a) and curve (b) to distinguish between site I and site II emissions. The labeled transitions start from the $^5D_0$ excited state and end at the levels indicated.

The non-degeneracy of the $^5D_0 \rightarrow {}^7F_0$ transitions at about 17,460 cm^{-1} and 17,360 cm^{-1} indicates the presence of crystallographically inequivalent sites. This is in accordance with the apatite lattice structure. Apatite has two inequivalent calcium sites: the Ca(I) site has C_3 symmetry, while the Ca(II) site has C_S symmetry [18]. The two different sites are henceforth called “site I” and “site II”. The corresponding excitation spectra are shown in Figure 4.

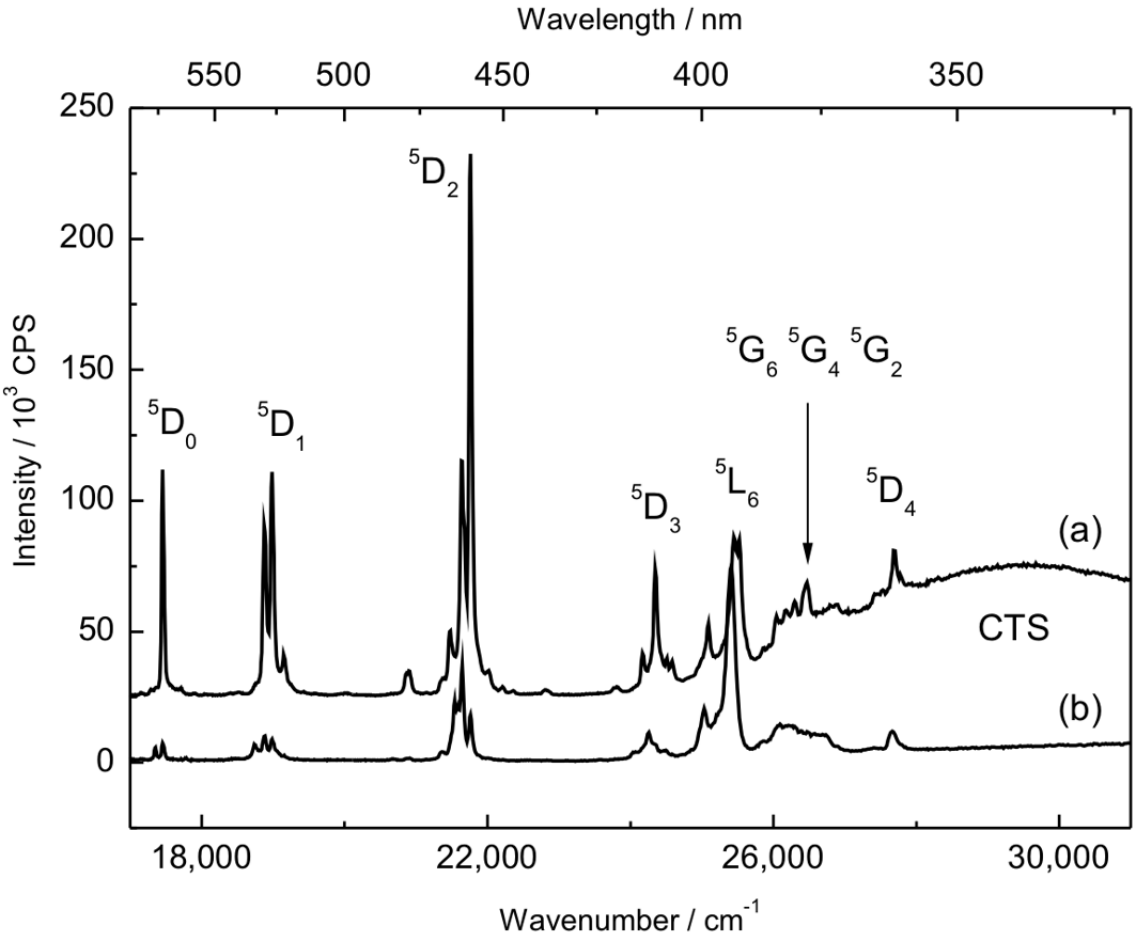

Figure 4. PL excitation spectra of $SiO_2/Ca_{10}(PO_4)_6OH:Eu^{3+}$ core-shell NPs sample (the doping concentration of Eu^{3+} is 2.5 mol%), recorded at (a) 15,936 cm^{-1} (627.5 nm – site I) and (b) 16,234 cm^{-1} (616.0 nm – site II). The labeled transitions start from the $^7F_0$ ground state and end at the levels indicated.

Apart from the typical, relatively narrow Eu^{3+}-related absorption bands, site I can be excited via so-called charge transfer state (CTS) absorption bands [17]. This CTS absorption band is relatively strong and has its maximum at approximately 340 nm. In 0.5 mol% Eu^{3+}-doped NPs [10], the CTS band can be found for both sites, site I and site II. The CTS band of site I is, however, much more intense than that for site II. Interestingly, the intensity ratio between the CTS band and the Eu^{3+} absorption bands is clearly in favor of the CTS band for the less doped NPs [10].

Upon excitation of the $^7F_0 \rightarrow {}^5L_6$ transition at 25,348 cm^{-1} (394.5 nm), both sites can be observed in the PL spectrum (see Figure 3, curve b); the two different sites cannot be spectrally resolved. However, if this spectrum is cleared from the site I emissions shown in Figure 3, curve a, the emissions of site II can be extracted (see Figure 3, curve c). Comparing the Eu^{3+} emissions of sites I and II, the $^5D_0 \rightarrow {}^7F_{1,2}$ emission of site II shows a blue shift and higher crystal field splitting; the $^5D_0 \rightarrow {}^7F_0$ emission of site II is, however, slightly red-shifted. Additionally, site II shows $^5D_0 \rightarrow {}^7F_{3,4}$ emission bands. Unfortunately, at room temperature, the analysis of the observed crystal field splitting for sites I and II did not allow an exact assignment to the corresponding lattice sites, as has already been described[19].

3.3. Optical properties of $SiO_2/Zn_2SiO_4:Mn^{2+}$ core-shell nanoparticles

In willemite the Mn^{2+} ions are situated at the slightly distorted tetrahedral sites with 4 oxygen neighbors [20]. In this case, the green room temperature luminescence, corresponding to the vibronic band of the spin-forbidden $^4T_1 - {}^6A_1$ transition, has its maximum at 525 nm with a bandwidth of about 40 nm (see Figure 5).

The applied excitation photon energy of 4.77 eV (260 nm) is smaller than the band gap of Zn_2SiO_4. The excitation of Mn^{2+} ions follows their ionization (transition from the ground state to the conduction band) and the non-radiative relaxation of the electrons to the excited state $^4T_1$ of Mn^{2+}. A fraction of the electrons can be trapped at nearby lattice defects, contributing to the afterglow of the Mn^{2+} emission observed in several samples. We measured the low-temperature PL spectra to find the zero-phonon lines (ZPLs) of the Mn^{2+} ions at two different lattice sites, observed by Stevels and Vink [21] in microcrystalline powders prepared by solid-state reactions. However, no ZPLs could be resolved in our samples at 18 K. This is probably due to the broad distribution of slightly distorted lattice sites leading to a high inhomogeneous

broadening of the ZPLs. Figure 5 shows the room-temperature spectra of two samples of $SiO_2/Zn_2SiO_4:Mn^{2+}$ NPs doped with 1 mol% and 20 mol% Mn^{2+}, annealed at 900 °C and one doped with 5 mol%, annealed at 1100 °C.

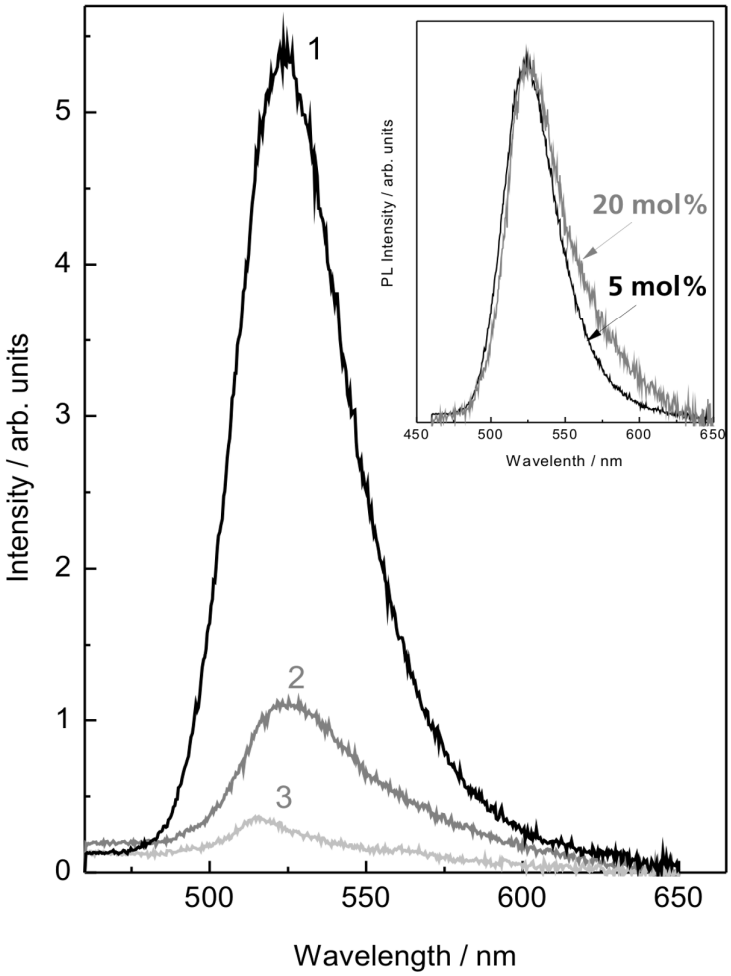

Figure 5. PL spectra of $SiO_2/Zn_2SiO_4:Mn^{2+}$ NPs doped with 1 mol% (curve 3) and 20 mol% Mn^{2+} (curve 2), annealed at 900 °C, and of the sample doped with 5 mol% (curve 1), annealed at 1100 °C. All spectra were recorded at RT under 260 nm excitation. Inset: normalized PL spectra of the samples doped with 5 mol% and 20 mol% Mn^{2+}.

By increasing the doping concentration from 1 mol% to 5 mol%, the luminescence intensity increases. At higher concentrations (20 mol%), luminescence efficiency is strongly affected by concentration quenching, as expected. The much stronger intensity of the 5 mol% sample in contrast to the 1 mol% and 20 mol% `samples can be explained by an additional effect. This sample was annealed at 1100 °C instead of 900 °C which results in a pure α-Zn_2SiO_4

phase with higher luminescence intensity, as reported elsewhere [9]. An annealing temperature of 900 °C is suboptimal and these samples contain a fraction of ZnO (see Figure 2). This is very probably related to the PL component with its maximum at 520 nm. The optimal doping concentration lies at about 5 mol% and the annealing temperature at 1100 ^{o}C. The inset in Figure 5 shows a comparison of the normalized spectra of the samples doped with 5 mol% and 20 mol% Mn^{2+}. The background emission has been subtracted for clarity. The difference seen in the red wing of the PL band is most likely due to the presence of pairs of manganese ions in the highly doped sample [22].

The broad red wing of the emission band is related to the emission of the Mn^{2+} pairs [22]. The effect of concentration quenching is especially well seen in the decay curves of the photoluminescence (see Figure 6). The sample with 1 mol% Mn^{2+}-doping has exponential PL decay with a lifetime of 17 milliseconds, characteristic for the forbidden Mn^{2+} d-d transitions in Zn_2SiO_4. A strong quenching is seen in the sample with 20 mol% doping. However, the clearly non-exponential decay curve can be fairly well described with the Inokuti-Hirayama equation with the radiative decay time similar to that of weakly doped samples and the energy transfer term corresponding to the quadrupole-quadrupole interaction. This equation is applicable in the case of missing or weak energy migration among the Mn^{2+} ions [23].

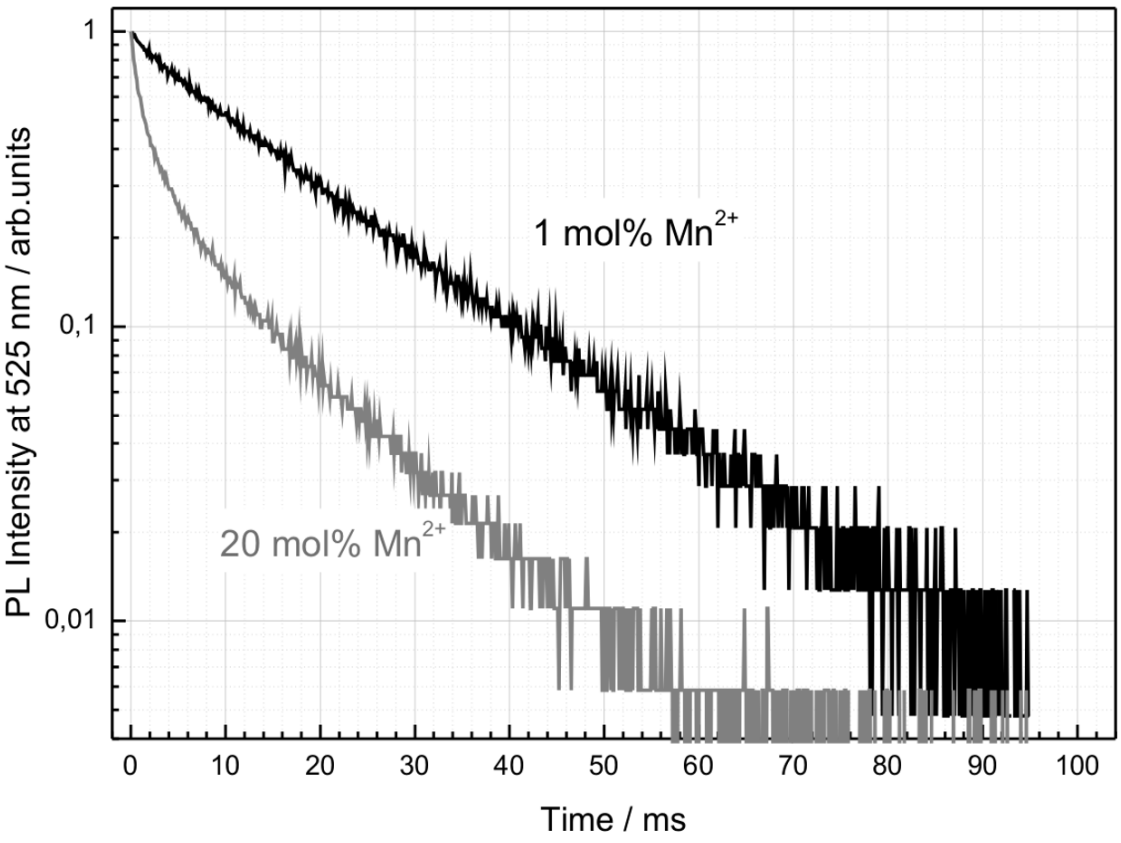

Figure 6. PL decay curves of $SiO_2/Zn_2SiO_4:Mn^{2+}$ samples with 1 mol% and 20 mol% Mn^{2+}.

4. Conclusion

Luminescent core-shell structured $SiO_2/Ca_{10}(PO_4)_6OH:Eu^{3+}$ and $SiO_2/Zn_2SiO_4:Mn^{2+}$ NPs labeled with different amounts of doping ions were successfully prepared via a sol-gel process followed by annealing at high temperatures. This study identified the relevance of the Eu^{3+} and Mn^{2+}-doping concentration for the luminescence properties of the $Ca_{10}(PO_4)_6OH$ and Zn_2SiO_4 shell, respectively. No influence on the crystal structure was detected for the $SiO_2/Ca_{10}(PO_4)_6OH:Eu^{3+}$ samples by variation of the doping ion fraction, whereas a different ratio of the ZnO to Zn_2SiO_4 phases was observed for $SiO_2/Zn_2SiO_4:Mn^{2+}$, depending on the Mn^{2+} concentration. Our results suggest that the presented synthesis method offers significant advantages for the fabrication of core-shell structured NPs. In this way, luminescent NPs on

the basis of inorganic materials with controlled structural and optical properties can be produced and will be suitable for various biotechnological applications.

Acknowledgement

This work was financially supported by the Fraunhofer-Gesellschaft zur Foerderung der angewandten Forschung e.V., Munich, Germany (Grant No. 692034 and 663662). We would also like to thank the Federal Ministry for Education and Research ("Bundesministerium für Bildung und Forschung") for their financial support within the Centre for Innovation Competence SiLi-nano® (Project No. 03Z2HN11). Authors also gratefully acknowledge Prof. Dr. G. Krohne (Biocenter, University of Wuerzburg, Germany) for the use of the electron microscopes.

References

[1] H. Chander, Mater. Sci. Eng., R 49 (2005) 113 – 155.

[2] H.A Höppe, Angew. Chem. Int. Ed. 48 (2009) 3572 – 3582.

[2] J. Shen, L.-D. Sun, C.-H. Yan, Dalton Trans. 42 (2008) 5687 – 5697.

[4] F. Caruso, in Colloids and Colloid Assemblies, Wiley-VCH, Weinheim 2004.

[5] R. Dittmeyer, R.W. Keim, G. Reysa, A. Oberholz in Chemische Technik:

Prozesse und Produkte. Band 2: Neue Technologie. Wiley-VCH, Weinheim 2004.

[6] B.M. Tissue, Chem. Mater. 10 (1998) 2837 – 2845.

[7] D.Y. Kong, M. Yu, C.K. Lin, X.M Liu, J. Lin, J. Fang, J. Electrochem. Soc. 152 (2005) H146 – H151.

[8] M. Yu, H. Wang, C.K. Lin, G.Z. Li, J. Lin, Nanotechnology 17 (2006) 3245 – 3252.

[9] S. Dembski, S. Rupp, C. Gellermann, M. Batentschuk, A. Osvet, A. Winnacker, J Colloid Interface Sci. (2010) submitted.

[10] S. Dembski, M. Milde, M. Dyrba, S. Schweizer, C. Gellermann, J. Mater. Chem. (2010) submitted.

[11] W. Stoeber, A. Fink, E. Bohn, J. Colloid Interface Sci. 26 (1968) 62 – 69.

[12] C. Gellermann, W. Storch, H. Wolter, J. Sol-Gel Sci. Technol. 8 (1997) 173 – 176.

[13] M. Milde, S. Dembski, C. Gellermann. M. Batentschuk, A. Osvet, manuscript in preparation.

[14] S.V. Dorozhkin, M. Epple, Angew. Chem. Int. Ed. 41 (2002) 3130 – 3146.

[15] M.A. Martins, C. Santos, M.M. Almeida, M.E.V. Costa, J. Colloid Interface Sci. 318 (2008) 210 – 216.

[16] R.P.S. Chakradhar, B.M. Nagabhushana, G.T. Chandrappa, K.P. Ramesh, J.L. Rao, J. Chem. Phys. 121 (2004) 10250 – 10259.

[17] X.Y. Chen, G.K. Liu, J. Solid State Chem. 178 (2005) 419 – 428.

[18] J.C. Elliott, R.M. Wilson, S.E.P. Dowker, Adv. X-Ray Anal. 45 (2001) 172 – 181.

[19] L. Binnemans, C. Görller-Walrand, J. Rare Earths 14 (1996) 173 – 180.

[20] S.R. Lucic, D.M. Petrovic, M.D. Dramicanin, M. Mitric, Lj. Dacanin, Scr. Mater. 58 (2008) 655 – 658.

[21] A.L.N. Stevels, A.T. Vink, J. Lumin. 8 (1974) 443 – 451.

[22] C.R. Ronda, T. Amrein, J. Lumin. 69 (1996) 245 – 248.

[23] B. Henderson, G.F. Imbusch, in Optical Spectroscopy of Inorganic Solids, Clarendon Press, Oxford 1989.